RESEARCH ARTICLE

The Role of Atmospheric Stability and Turbulence in Offshore Wind-Farm Wakes in the German Bight

Andreas Platis[1] · Marie Hundhausen[2] · Astrid Lampert[3] · Stefan Emeis[4] ·
Jens Bange[1]

Abstract

Airborne meteorological in situ measurements as well as stationary measurements at the offshore masts FINO1 and FINO3 in the German Bight are evaluated in order to examine the hypothesis that the wake dissipation downstream of large offshore wind farms depends on atmospheric stability. A long-term study of the mast data for the years 2016 and 2017 demonstrates a clear dependence of stability on the wind direction. Stable conditions are predominantly expected during southerly winds coming from the land. The analysis of various stability and turbulence criteria shows that the lapse rate is the most robust parameter for stability classification in the German Bight, but further implies that stability depends on the measurement height. A near-surface (0 to 30 m), predominantly convective, layer is present and more stable conditions are found aloft (55 to 95 m). Combing the stability data with the airborne measurements of the offshore wind-farm wakes reveals the trend of a correlation between longer wake lengths and an increase in the initial wind-speed deficit downwind of a wind farm with stronger thermal stability. However, the stability correlation criteria with the wake length downstream of the four investigated wind farms, Godewind, Amrumbank West,

✉ Andreas Platis
  andreas.platis@uni-tuebingen.de

  Marie Hundhausen
  marie.hundhausen@kit.edu

  Astrid Lampert
  astrid.lampert@tu-braunschweig.de

  Stefan Emeis
  stefan.emeis@kit.edu

  Jens Bange
  jens.bange@uni-tuebingen.de

[1] University of Tübingen, Environmental Physics Group, GUZ, Schnarrenbergstr. 94-96, 72076 Tübingen, Germany

[2] Institute for Meteorology and Climate Research (IMK-TRO), Karlsruhe Institute of Technology (KIT) Hermann-von-Helmholtz-Platz, 1, 76344, Eggenstein Leopoldshafen, Germany

[3] Institute of Flight Guidance, TU Braunschweig, Hermann-Blenk-Str. 27, 38108, Braunschweig, Germany

[4] Institute for Meteorology and Climate Research (IMK-IFU), Karlsruhe Institute of Technology (KIT) Kreuzeckbahnstr, 19 82467, Garmisch-Partenkirchen, Germany

Springer

Meerwind Süd/Ost, and Nordsee Ost, contain large variance. It is assumed that the observed scattering is due to the influence of the wind-farm architecture and temperature inversions around hub height. These, however, are crucial for the classification of stability and illustrate the complexity of a clear stability metric.

1 Introduction

Compared to onshore sites, the offshore installation of wind turbines is favourable due to higher wind speeds, a lower level of turbulence, and large available areas (Henderson et al. 2003). Therefore, with the rapid deployment of wind energy, an increasing portion of turbines are installed offshore. For optimal area use and in order to minimize costs for infrastructure, offshore wind turbines are clustered into large wind farms.

Due to the extraction of kinetic energy from the flow, each turbine generates a wake that is characterized by a decrease in wind speed and increased level of turbulence (Barthelmie et al. 2010). Within a wind farm, individual wakes merge with the with wakes from neighbouring turbines forms a downstream wake (Emeis 2018).

As revealed by observations from synthetic aperture radar on a satellite, wakes downstream of offshore wind farms can exceed several tens of kilometres (Christiansen and Hasager 2005; Djath et al. 2018). Moreover, the first analysis of airborne in situ measurements shows reductions of the flow field up to 70 km downstream of the wind farm in certain atmospheric conditions (Platis et al. 2018). It is thus expected that such large wakes affect farms located downstream, as already observed by Nygaard (2014) and Nygaard and Hansen (2016). From an economic point of view and for the successful planning of further offshore farms, it is therefore crucial to identify the meteorological parameters that affect wake development.

Following the explanation by Barthelmie and Jensen (2010), the development of the wake and the wake recovery depend on atmospheric stability: during convective conditions, which are associated with enhanced mixing and a high turbulence intensity, an increased transfer of momentum rapidly erodes the wind-speed deficit in the wake. In contrast, during stable conditions, where mixing is inhibited, the wake dissipation is inhibited. Consequently, wakes are expected to be especially pronounced at offshore locations, where, compared with onshore sites, low surface roughness and thus low turbulence intensities are present (Hansen et al. 2012; Emeis et al. 2016). The effect of stability on the wake dissipation was analytically derived in Emeis (2010). In field measurements, evidence for a correlation of atmospheric stability and wake intensity is found for example by Magnusson and Smedman (1994), Hansen et al. (2012), Rhodes and Lundquist (2013), Peña et al. (2014) and Krishnamurthy et al. (2017), who show a decrease of the wind-farm efficiency with more stable conditions. The first distinct relationship between stability and the wake length using synthetic aperture radar data of a wind farm far field was identified by Djath et al. (2018), showing that at the wind farm Alpha Ventus in the German Bight, the wake length increases with stronger lapse rate, and could be described by a linear function. Platis et al. (2018), Cañadillas et al. (2019) and Platis et al. (2021) used in situ measurements to show that stable conditions favour longer wakes, though, only case studies are presented.

This study comprises the analysis of a unique dataset of 41 in situ flight measurements in the vicinity of offshore wind farms in the German Bight (Platis et al. 2020) and measurements

from the FINO1 and FINO3 masts in order to investigate systematically the relationship between stability and wake.

Three major questions are addressed. In Sect. 4.1, a long-term analysis of the stability in the German Bight is done using stationary FINO data. Secondly, in Sect. 4.2, a comparison of stability measures from FINO data and aircraft measurements is conducted, and the strengths and weaknesses of the parameters and measurement techniques are presented. We discuss which parameters are most representative of stability in the German Bight, aiming to identify which measure is most useful for describing stability at an offshore wind farm. Section 4.3 covers the analysis of the stability and its influence on the wake extension. Stability is established in relation to the wake length and initial wind-speed deficit to test the hypothesis of a correlation between stability and wake intensity.

2 Stability and Turbulence Measures

Atmospheric stability describes the potential of vertical motion of air. A layer is considered as stable when vertical motion is suppressed and as unstable or convective when vertical motion is enhanced (Stull 1988). The two concepts of stability are static stability, which takes solely buoyancy into account and dynamic stability, which also considers shear-generated turbulence.

Static stability is measured by the gradient of virtual potential temperature θ_v with the height z, named the lapse rate γ. For the lapse rate, no turbulence measurements are necessary since only mean differences and height mean differences in temperature are required:

$$\gamma = \frac{d\theta_v}{dz} \approx \frac{\Delta\theta_v}{\Delta z}. \tag{1}$$

The lapse rate is negative during convective conditions, zero for neutral, and positive for stable cases.

Dynamic stability is commonly described by the bulk Richardson number Ri_B and is based on mean measures only. It is calculated according to

$$Ri_B = \frac{g\,\Delta\overline{\theta_v}\,\Delta z}{\overline{\theta_v}\,\Delta\overline{U}^2} \tag{2}$$

where g is the acceleration due to gravity, and U is the wind speed. The overbar represents a mean value. Stable conditions are expected when $Ri_B > 1$ and convective or turbulent conditions when $Ri_B < 0.25$ (Stull 1988), see Table 1. However, those thresholds are valid for local gradients only and deviate with larger height intervals $1z$ (e.g., Stull 1988; Balsley et al. 2008).

An alternative method for dynamic stability that does require turbulence measurements is described by the Obukhov length

$$L = \frac{-\overline{\theta_v}u_\star^3}{\kappa g\left(\overline{w'\theta_v'}\right)}, \tag{3}$$

with

$$u_\star = \left(\left(\overline{u'w'}\right)^2 + \left(\overline{v'w'}\right)^2\right)^{\frac{1}{4}}, \tag{4}$$

where $\kappa \approx 0.4$ is the von Kármán constant (Stull [1988]), and $u_\star$ is the friction velocity, which can be derived from the turbulent parts of the wind components u, v, and w, marked by a prime (Eq. [4]); u is defined northwards, v eastwards, and w is the vertical component, positive upwards. The flux $\overline{w'\theta_v'}$ describes the turbulent kinematic heat flux. Since the airborne measurements used for the derivation of the heat flux and $u_\star$ were performed at hub height, in our dataset, L is considered as a local metric at this height. Often the Monin–Obukhov stability parameter ζ with the measurement height z is evaluated,

$$\zeta = \frac{z}{L}, \tag{5}$$

with negative ζ indicating convective conditions, whereas positive ζ defines stable conditions. However, the calculation requires high-frequency measurements of the turbulent wind components and virtual potential temperature differences.

Moreover, there are several parameters that quantify turbulence. Most prominent is the turbulence kinetic energy (e) per unit mass

$$e = \frac{1}{2}\left(\overline{u'^2} + \overline{v'^2} + \overline{w'^2}\right). \tag{6}$$

Offshore, Archer et al. ([2016]) observed that e varies between 0.1 to $10\,\text{m}^2\,\text{s}^{-2}$ and increases with the wind speed at 20-m height. Lidar observations by Bodini et al. ([2019]) reveal that the dissipation rate—which can be derived from the value of e—is on average smaller compared with onshore conditions. However, a relationship between increasing atmospheric stability and decreasing e, as determined in Wharton and Lundquist ([2012]) over land, has not been documented in the literature as far as we know.

In some studies the variance of the vertical velocity component $\overline{w'w'}$ alone is also considered as a turbulence criterion. Türk and Emeis ([2010]) observed that this quantity depends mainly on wind speed and is only influenced to a small extent by atmospheric stability.

The turbulence intensity I [%] is defined as the standard deviation of the wind speed, normalized by the mean wind speed,

$$I = 100\,\frac{\sigma_U}{\overline{U}}. \tag{7}$$

Offshore, the value of I is observed around 4 to 5 % during stable conditions, and increases to about 7 % as the atmosphere becomes more unstable (Hansen et al. [2012]). However, also a significant correlation with wind speed was identified and a dependence on the wind direction indicates that the thresholds are site specific.

An overview of the stability classification for the prevalent criteria is provided in Table [1].

3 Method

3.1 Data Acquisition

The study is based on two datasets. First, meteorological long-term data recorded by the permanent measurement masts FINO1 and FINO3 are used (Fig. [1]). The masts are equipped with various meteorological sensors for recording the wind speed, temperature, and humidity at the heights of 30, 40, 50, 70, and 90 m for FINO1 (Table [2]) and in 29, 55, and 95 m for FINO3 (Table [2]). Routine meteorological data are stored as 10-min averages, sea surface temperature every 30 min. Virtual potential temperature θ_v is calculated for all the sensor

Table 1 Overview of offshore stability classification. References (Ref.) are: (1) Camuffo (2014), (2) Stull (1988), (3) Van Wijk et al. (1990), Muñoz-Esparza et al. (2012) (4) Hansen et al. (2012), and (5) Wharton and Lundquist (2010)

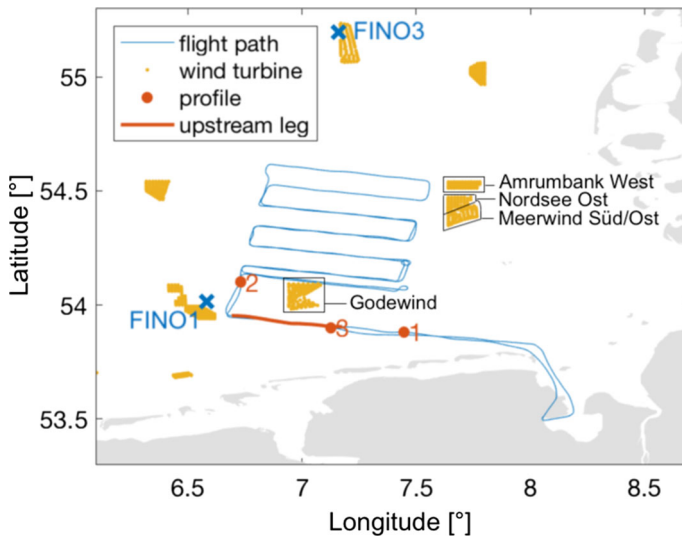| Parameter	Very stable	Stable	Neutral	Convective	Very convective	Ref.
γ (K m^{-1})	> 0		≈ 0	< 0		(1)
Ri_B	> 1			< 0.25		(2)
L (m)	0 to 200	200 to 1000	$|L| > 1000$	-1000 to -200	-200 to 0	(3)
$\zeta(z = 80$ m$)$	> 0.4	0.08 to 0.04	$|\zeta| < 0.08$	-0.4 to 0.08	< -0.4	(4)
I (%) offshore	≈ 4			≈ 7		(4)
e (m^2 s^{-2}) onshore	< 0.4	0.4 to 0.6	0.6 to 1	1 to 1.4	> 1.4	(5)

Fig. 1 The visualization of the field site in the German Bight, showing the wind farms, measurement masts, and an example flight path on 15 October 2017 (flight 41). Map material: OpenStreetMap (2017)

Table 2 Measurement heights at FINO masts, where ϕ is the wind direction, T is the temperature

FINO1 Height in m	20	30	33	40	50	60	70	80	90	100
T		×		×	×		×			×
p	×								×	
RH			×	×			×		×	
U			×	×	×	×	×	×	×	×
ϕ			×	×	×	×	×	×	×	

FINO3 Height in m	23	28	29	30	40	50	55	60	70	80	90	94	95	100	106
T			×				×						×		
p	×											×			
RH			×				×						×		
U				×	×	×		×	×	×	×			×	×
ϕ		×						×						×	

heights. To ensure an accurate lapse-rate calculation, the temperature sensors at both masts have been undergoing a relative calibration process (Frühmann 2016).

The quantities of pressure p, relative humidity RH, wind speed, and direction are linearly interpolated to the height of interest if not available. Moreover, RH is assumed to be 100 % at the water surface (0 m). For θ_v at the water surface, the temperature is derived from the water temperature measurement of the buoy similar to the method by Foreman et al. (2017) who used the sea surface as a proxy for the lapse-rate calculation. Data are averaged over a 10-min period, which is identical to the airborne measurements. Sonic anemometers at FINO1 at a

height of 40 and 80 m provide 20-Hz frequency data of the wind velocity components as well as the sonic temperature T_s. More details can be found in Foreman et al. (2017).

Also analyzed are airborne meteorological measurements conducted in the research project WIPAFF (Platis et al. 2020, WInd PArk Far Field) comprising four field campaigns from September 2016 to October 2017 for a total of 41 measurement flights. The measurements were made from the research aircraft Dornier DO-128 operated by the Technische Universitt Braunschweig. The aircraft is equipped with sensors for temperature, humidity, pressure, and wind components, sampling at a frequency of 100 Hz. Details about the measurement devices can be found in Corsmeier et al. (2001), Platis et al. (2018), and Lampert et al. (2020). The airspeed of the research aircraft is $66 \, \mathrm{m \, s^{-1}}$. The airborne flight data are publicly available (Bärfuss et al. 2019).

All flights were conducted in the German Bight, in the vicinity of an operating offshore wind farm either Godewind (GO) or the cluster with the wind farms belonging to the Amrumbank West Cluster: Amrumbank West (AW), Nordsee Ost (NO), and Meerwind Süd-Ost (MSO). A typical flight pattern (Fig. 1) comprises the following features: upwind of the wind farm, with a distance of approximately 5 km to the turbines, there is one leg perpendicular to the flow (red) to measure the undisturbed flow. Downwind of the wind farm, the legs are arranged in a meander pattern. Whereas the first leg has a distance of about 1 km to the farm, the farther downstream legs follow with a spacing of 10 km. The legs usually have a length of 40 km, which corresponds to a flight time of 10 min.

The approximate height of the pattern is at about 100 m adjusted to the turbine hub height. Furthermore, vertical profiles between 30 to 1000 m are flown in the vicinity of the wind farm (numbered in Fig. 1) and used for the vertical probing of the lower atmosphere.

3.2 Stability Characterization

Stability is analyzed according to the parameters presented in Sect. 2. Starting with the gradient based criteria γ and Ri_B, those are calculated over a number of different height intervals.

For the long-term analysis of γ at the FINO measurement masts, the gradient is calculated from the measurements at two heights each. For the FINO1 mast, the gradients are 0–95 m, 29–95 m, and 55–95 m and 0–90 m, 33–90 m, and 50–90 m for the FINO3 mast; this is to calculate the stability in relation to the wind-turbine hub height at about 100 m. For the aircraft measurements the gradients are 50–100 m, 30–150 m, and 60–120 m extracted from the vertical profiles. For each case, the gradients of θ_v and U are calculated using the vertical flight sections by the aircraft measurements and a linear regression within the height range for the FINO mast data. If the vertical flight section does not cover the entire altitude range, the flight is ignored. The vertical probing by the aircraft took about 10–15 min. The observed stability parameters at the FINO masts are evaluated at the same time as the flight profiles, using the 10-min time-average mast measurement closest to the flight time, thus tower measurements and aircraft measurements always overlap. For one measurement flight, the lapse rate γ is calculated using the arithmetic mean, and Ri_B using the median due to present outliers. For the FINO masts, the regression is calculated over all available measurement heights in the height interval.

The parameters ζ, I, e, $\overline{w'\theta_v'}$, and $\overline{w'w'}$ are calculated as described in Sect. 2 using high-frequency data of the first undisturbed flight leg and over a time span of 10 min at FINO1 at a height of 80 m. Due to distortion from the measurement tower as well as the adjacent wind farm Alpha Ventus, FINO1 data are only evaluated for a wind direction $\phi > 180°$ (Foreman

Fig. 2 Example wind-speed contour plot of flight 7 on 10 September 2016 downstream of the Amrumbank West cluster, adapted from Platis et al. (2018). The wake area is defined between the solid grey boundaries and the undisturbed zone is bounded by dashed lines
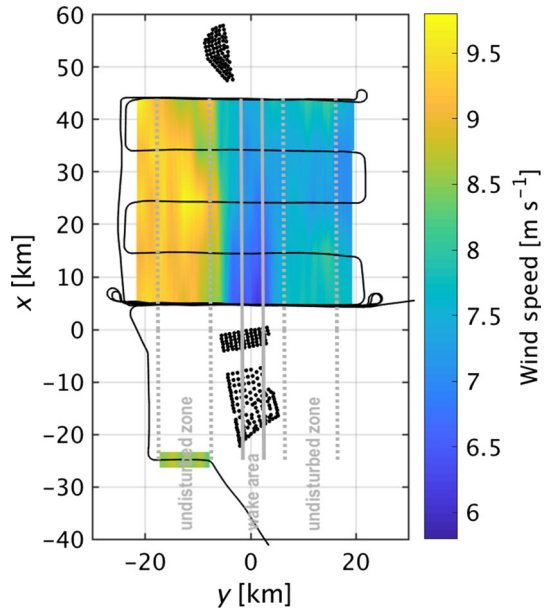
et al. 2017). Furthermore, filtering of the sonic data is done based on Cañadillas et al. (2011), applying a cut-in and cut-off of $-15\,°C$ to $30\,°C$ for T_s, $-15\,\mathrm{m\,s^{-1}}$ to $15\,\mathrm{m\,s^{-1}}$ for w, and a limit of $35\,\mathrm{m\,s^{-1}}$ for U.

3.3 Wake Characterization

For processing the wake measurements, the flight pattern is projected to Cartesian coordinates with the flow coming from negative x (Fig. 2) and its origin at the farthest downstream-located wind turbine of the farm. We use the method introduced by Platis et al. (2020). The wake region is determined manually, with the choice of a left and right boundary of the region of significantly reduced wind speed, and is extended linearly along the mean wind direction, as visualized for flight 7 in Fig. 2. Moreover, this example shows that in some cases the background wind speed is inhomogeneous (higher wind speeds left of the wake in the direction of flow). Such inhomogeneities are mainly attributed to mesoscale wind patterns and the effect is aimed to be minimized by averaging over an adequately wide undisturbed area on both sides of the wake, which is why the upstream leg is not used as a reference. Therefore, the undisturbed zone is defined left and right of the wake using a distance of 4 km as buffer zone between wake and undisturbed area and a width of 10 km to both sides. However, these default distances are adapted if required for example due to wind directions not perpendicular to the flight pattern, asymmetric patterns, or strong spatial inhomogeneities. In case distinct wakes build up behind the different wind farms of the cluster, several wake areas are defined.

The extent of the wake is defined by the relative wind-speed deficit D_r in the mean wind direction,

$$D_r(x) = \frac{u_f(x) - u_r(x)}{u_f(x)},$$ (8)

Table 3 Long-term stability evaluated over the lapse rate γ at FINO1 and FINO3 for 2016 and 2017

Mast	Height (m)	% Data availability	% Convective	% Stable
FINO3	0–95	79	71	29
	29–95	88	61	39
	55–95	94	12	88
FINO1	0–90	70	69	31
	33–90	68	41	59
	50–90	86	37	62

with u_r the averaged wind speed in the wake zone, and u_f the averaged wind speed in the undisturbed zone, both as a function of the downwind coordinate x as in some cases significant gradients within the background wind speed are observed for flow from the land. Similar observations are made in previous studies (Christiansen and Hasager 2005; Djath et al. 2018). The end of a wake is defined as the downstream distance at which $D_r(x) < 5\,\%$. Furthermore, the wake can be characterized in time t and having a wake duration t_{95}, with $D(t_{95}) < 5\%$ when the expression is transferred into the time domain

$$D_r(t) = \frac{u_f(t) - u_r(t)}{u_f(t)}, \quad \text{with} \quad t = \frac{x}{\overline{u_r(x)}}. \tag{9}$$

Here, $\overline{u_r(x)}$ is the average wind speed within the wake over all downstream legs. This is assumed to be the best approximation of the speed of a travelling air parcel within the wake and is therefore taken as the characteristic speed. The third wake parameter is the initial velocity deficit D_{r1}, which is obtained as D_r of the first flight leg downwind of the wind farm at $x = 1$ km.

4 Results and Discussion

4.1 Long-Term-Stability Analysis in the German Bight

To assess the stability conditions at offshore wind farms in the German Bight, a long-term study of the lapse rate γ is conducted, comprising the years 2016 and 2017. This choice is based on the high data availability during this period. We analyzed all situations with wind speeds between 5 and 25 m s^{-1} at 90 m. The lapse rate γ is calculated between different measurement heights with respect to the maximum height at the FINO masts, which refers to the hub height at about 100 m. The lower heights are defined by the altitude of the thermometers at the masts (Table 2).

Starting with the FINO3 mast, which is located farther offshore and further away from wind farms, the height intervals are 55–95 m, 29–95 m, and 0–95 m. Data availability decreases from 95–79 % with the height range (Table 3).

The histogram of the probability distribution of γ (Fig. 3a) shows that the gradient for the 29 and 55–95 m interval ranges from about -0.01 to 0.02 K m^{-1}. The distribution is narrow and has a distinct peak around zero, which is slightly shifted towards negative (unstable) values for 29–95 m (yellow) and towards positive (stable) for 55–95 m (blue). Moreover, both distributions are skewed to the right. The sea-surface temperature varies slowly compared
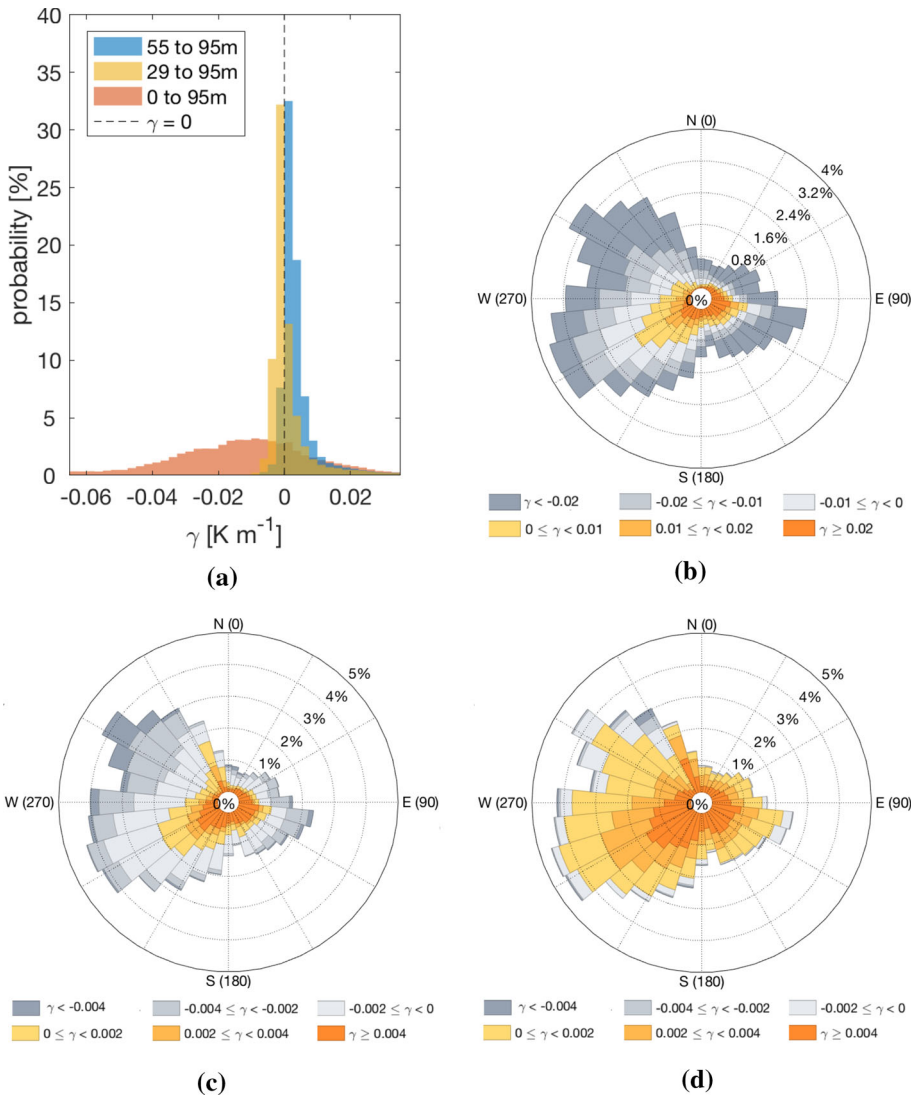
(a)

(b)

(c)

(d)

Fig. 3 Evaluation of the lapse rate, γ, at the FINO3 mast for 2016 and 2017 and stability roses of γ measured at the FINO3 mast over alternative height intervals. **a** Histogram of the γ distribution depending on different altitude intervals. **b** Stability rose displaying γ as the variable for the altitudes 0–95 m as a function of wind direction. **c** Stability rose displaying γ as the variable for the height interval 30–95 m. **d** Stability rose displaying γ as the variable for the height interval 55–95 m

with the air temperature and the gradient of 0–95 m results in a significantly wider distribution, ranging from -0.06–$0.03\,\mathrm{K\,m^{-1}}$. The mode is at $-0.01\,\mathrm{K\,m^{-1}}$.

The higher the height range that the gradient calculation is located, the more the distribution is shifted towards larger γ values, and therefore more stable conditions, similar to the findings by Argyle and Watson (2014). As listed in Table 3, with the use of the sea-surface temperature the minority with only 29 % are classified as stable for at the FINO3 mast. Using the highest altitude interval (55 to 95 m) the majority is stable with 88 %.
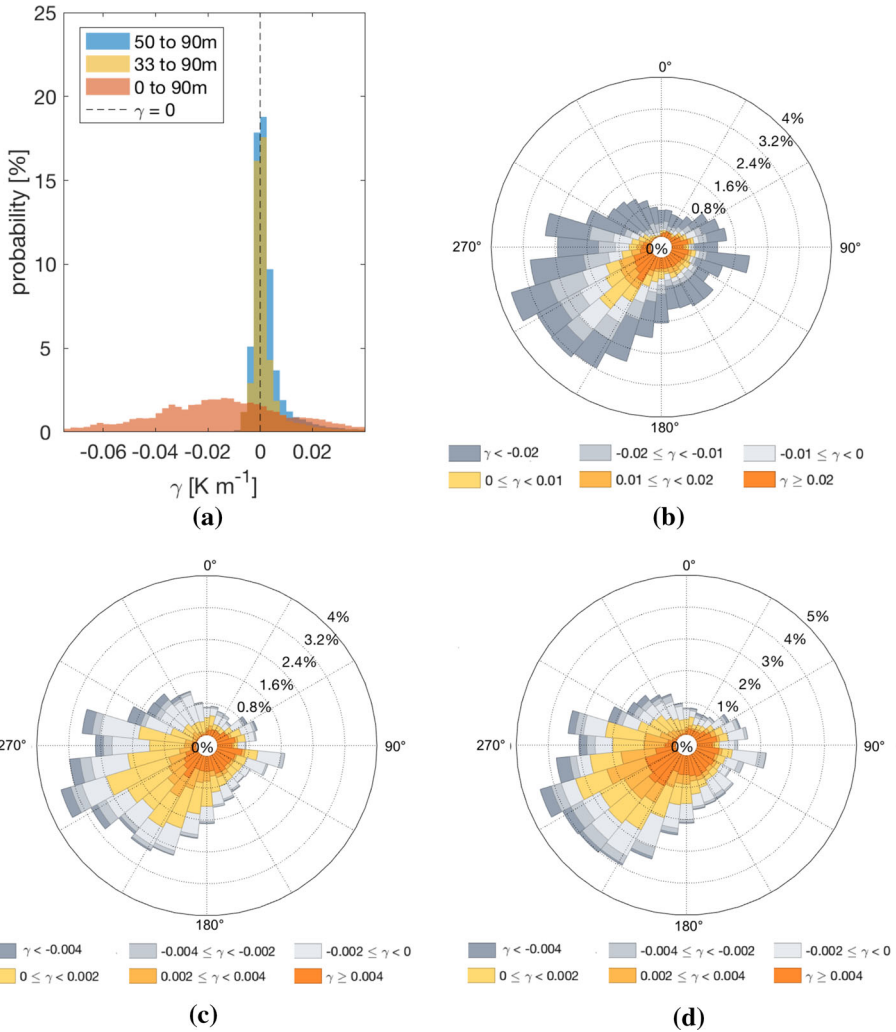
Fig. 4 As for Fig. 3 but for the FINO1 mast

In Fig. 3a and b the distribution of γ according to the wind direction is represented for the calculation of γ over 0–95 m. However, the key features of the stability rose can be revealed even more clearly if two alternative vertical separation heights (between 30–90/95 and 50–90/95 m) are considered (Fig. 3c and d). According to the stability rose, there is an asymmetric distribution. For flow from the from north-west to north-east, the percentage of stable cases is very low. During winds with a southern component, stable cases become more relevant. The variation of the vertical separations reveals additionally how sensitive the choice of the height interval is on the stability determination.

The analysis of the FINO1 data largely supports the findings (Fig. 4). In general, the data availability is lower than for the FINO3 data with 75 % on average. As above, three different altitude intervals are evaluated: 0–90 m, 33–90 m, and 50–90 m. Depending on the altitude interval, the same trend is visible as for the FINO3 mast: the higher the lower measurement

point, the larger the percentage of stable situations (Table 3). The influence of height intervals on the lapse rate measured by the FINO masts is further discussed in Sect. 4.3 for the time of WIPAFF flight cases. Further, results confirm the observed trend.

Moreover, γ shows dependence on the wind direction (Fig. 4f–h), resembling the findings at the FINO3 mast. Most of the stable situations are observed during winds with a southern component. Especially for south-west winds, a percentage of stable cases up to 47 % is found.

4.1.1 Comparison and Discussion

According to the analysis in Sect. 4.1, the highest percentage of stable conditions in the German Bight is expected for flow from land from the south. In contrast, for the flow from open sea from the northern direction, the conditions are predominantly convective. The presented results fit well in the framework of existing studies of the dynamic stability parameters in the German Bight (Westerhellweg et al. 2010; Sathe 2010; Emeis et al. 2016; Platis et al. 2021). As outlined in Emeis et al. (2016), this behaviour is typical over the ocean for the northern hemisphere in the temperate westerly wind belts: warm sector winds most frequently come from the south-west and are thus followed by rather stable conditions, whereas cold sector winds come from the north-west and predominantly bring convective conditions. However, compared to the theory proposed by Emeis et al. (2016), the sector of most stable conditions in our dataset is shifted towards the south or even south-east. An explanation is that land mass in the south and south-east has an impact on the stability conditions as warm air masses over the land are advected over the sea during noon and afternoon. Moreover, as mentioned already in Sect. 3.2, also the wind farms adjacent to the measurement masts (Alpha Ventus next to FINO1 and Dan Tysk east of FINO3, see Fig. 1) alter the analysis (Foreman et al. 2017). However, it is difficult to assess whether the adjacent wind farms alter the stability observations on a long-term perspective. According to Siedersleben et al. (2018), temperature changes in the order of 0.5 to 1 K have been observed in the wake during stable conditions at hub height. This warming may lead to an even stronger gradient between sea surface temperature and hub height, thus to a stronger stability during thermal stable cases.

The stability classification according to γ depends crucially on the measurement altitude. The trend is observed that the lower the lowest measurement point for the gradient calculation, the more convective cases are expected. One reason might be frequent cases with unstable stratification close to the water surface. The hypothesis is supported by Argyle and Watson (2014) for example, concluding from an analysis of L that the marine air below 50 m is mostly very unstable compared to the stronger stability above, suggesting the presence of an internal marine boundary layer.

Concerning the measurement location, the FINO1 mast is located closer to the shore than the FINO3 mast and is expected to be more influenced by the land mass. The FINO1 data reveal the percentage of stable cases higher for the intervals 0 to 90 m and 33 to 90 m compared with the two corresponding intervals at the FINO3 mast. In contrast, the estimated percentage is lower for the interval 50 to 90 m compared to the respective interval at FINO3. The finding indicates that for the different height intervals, the FINO1 data reveal results in more homogeneous values of stability compared with at the FINO3 mast.

### 4.2 Evaluation of Stability and Turbulence Criteria Using Flight and FINO Data

The comparison of the criteria γ, Ri_B, ζ, I, e, $\overline{w'w'}$, and $\overline{w'\theta_v'}$ illustrated with the help of the Spearman rank correlation coefficient r (e.g., Sachs 2013) is provided in Table 4 (full list of

Table 4 Spearman rank correlation coefficients in % calculated between the criteria in the column and the row header

		γ	Ri_B		e		I		$\overline{w'w'}$		$\overline{w'\theta'_v}$		ζ	
		F1/3	AC	F1/3	AC	F1	AC	F1	AC	F1	AC	F1	AC	F1
γ	AC	**78**	61	32	−22	−1	−58	−14	−68	−10	−69	24	−3	−26
	F1/3		52	57	−47	−4	−77	−4	−76	−31	−66	−3	−9	14
Ri_B	AC	52		**30**	−34	13	−7	19	−55	1	−33	6	−69	−18
	F1/3	57	**30**		−5	6	−46	16	−3	−22	−3	−12	−19	13
e	AC	−47	−34	−5			52		53		29		1	
	F1	−4	13	6				64		93		1		−8
I	AC	−77	−7	−46	52				32		42		−24	
	F1	−4	19	16		64				55		−8		17
$\overline{w'w'}$	AC	−76	−55	−3	53		32				64		−15	
	F1	−31	1	−22		93		55				17		−23
$\overline{w'\theta'_v}$	AC	−66	−33	−3	29		42		64				−59	
	F1	−3	6	−12		1		−8		17				−77
ζ	AC	−9	−69	−19	1		−24		−15		−59			
	F1	14	−18	13		−8		17		−23		−77		

High correlation is marked by 100%, no correlation by 0 and high anti-correlation −100%. Each criterion comprises the results of the available measurement flights or the according FINO data. The term F1/3 indicates that FINO1 results are used when the flight was conducted at Godewind and FINO3 for the Amrumbank West cluster. AC abbreviates aircraft measurement. The gradient-based criteria are evaluated between 50 and 100 m. The comparison of gradient-based and turbulence-based stability criteria for the flight is only conducted for flights with an undisturbed leg measured at 100 m a.s.l. For empty fields, denoted with "−", no data for comparison are available due to a deviating aircraft altitude

Fig. 5 Scatter plot of the lapse rate for the 50–100 m height interval from the flights and FINO1/3 with the standard deviation between the single profile measurements during one measurement flight as the error bars. The FINO measurements closer to the flight path are plotted in colour, and in grey for the alternative FINO measurements. For better clarity, error bars are pictured for the FINO mast closer to the flight measurement only; GO and AW denote the Godewind and Amrumbank West wind farms
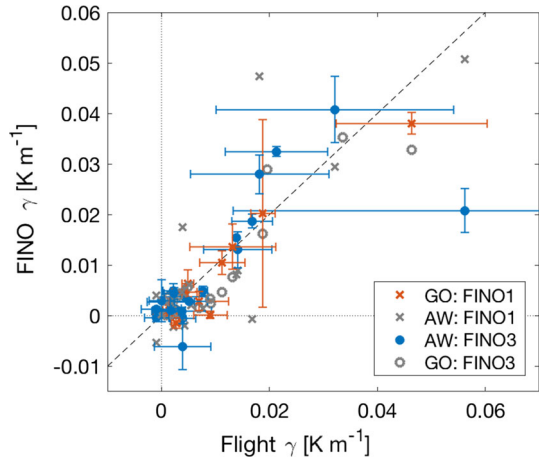
stability output is given in Tables 6 and 7). With this coefficient, the strength and direction of association between two variables is measured without assuming a linear relationship as with the Pearson correlation coefficient. Gradient-based parameters are evaluated in the interval of 50 to 100 m for aircraft and FINO measurements to assure comparability. A crucial feature that must be taken into consideration is that parameters such as γ and Ri_B are obtained within a layer and others, such as ζ and its input variable $\overline{w'\theta'_v}$ or the turbulent quantities, are obtained only for a certain height. We further discuss the consequences of this issue at the end of Sect. 4.2.2. The following explains the Table 4 with visualizations and discussions of the most promising as well as unexpected results.

4.2.1 Comparison of Different Measurement Locations

For the correlation between the same criteria evaluated at different locations, as shown in bold in Table 4, the results of FINO1 and FINO3 masts are condensed using only the measurement mast closest to the flight measurement (FINO1 for flights at Godewind and FINO3 at the Amrumbank West cluster). No comparison is conducted of FINO1 and flights for the turbulence-based measures due to deviating measurement heights.

The lapse rate γ shows the highest correlation coefficients between aircraft and FINO data of 78% and is shown as a scatter plot in Fig. 5. The error bar indicates the standard deviation between the airborne-measured profiles if several consecutive profiles were flown. The gradient ranges from -0.004 to about $0.06 \, \text{K m}^{-1}$ with an accumulation of cases between 0 and $0.01 \, \text{K m}^{-1}$. There is adequate agreement with the dashed bisecting line. The root-mean-square error (r.m.s.e.) between the two datasets is $0.008 \, \text{K m}^{-1}$, which is due to the spatial separation of the measurement readings by several tens of kilometres. Furthermore, it should be noted that during strong stability especially the uncertainty is larger, as seen by larger error bars, mainly caused by a fluctuating height of the inversion top that crucially influences the slope of the regression. By trend, the error in γ evaluated at FINO masts is smaller than for the flight, indicating that the spatial and temporal variability between the single flight profiles contributes to the uncertainty.

To estimate the effect of the spatial variability of the temperature gradient in the German Bight, the simultaneous results of the two measurement masts FINO1 and FINO3, which are separated by a distance of about 130 km, are compared (Fig. 6). With $r = 55\%$, the

Fig. 6 Scatter plot of the lapse rate measured at the FINO1 and FINO3 masts, with the standard deviation between the profile measurements as the error bars
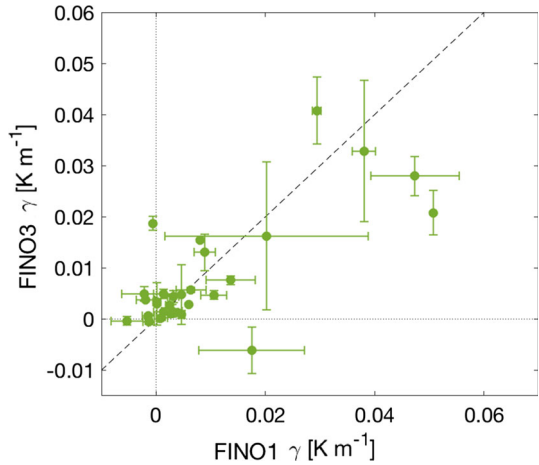
correlation is lower and a significant deviation from the bisecting line is observed, especially at high stability.

The Richardson number Ri_B is evaluated over a gradient-based method (not shown) but results in a far smaller correlation coefficient of 30 % between the flight and FINO measurements. In both datasets there is a high variability with several outliers and no functional relationship could be observed.

4.2.2 Comparison of Different Stability Criteria at the Same Location

This section is dedicated to a comparison of the different stability criteria during the same atmospheric conditions at the same location. The expected relationship between the stability criteria and turbulence measurements is a negative correlation: when the stability increases (increasing γ, Ri_B, or ζ), the turbulent quantity decreases (decreasing e, I or $\overline{w'w'}$).

Different measurement heights are considered by the different stability parameters. Whereas γ and Ri_B are obtained within a layer with vertical separation from 50–100 m above sea level (a.s.l), ζ and its input variable $\overline{w'\theta'_v}$ are recorded only at one distinct height at 100 m a.s.l.

One of the highest correlations between a gradient-based stability criterion and a turbulence criterion of the flight measurement with $r = -68$ % is found for the lapse rate γ with the variance of the vertical velocity component (Fig. 7a). The plot reveals that during thermal instability, indicated by a negative or near-zero temperature gradient, the amplitude of $\overline{w'w'}$ is high. With increasing γ, $\overline{w'w'}$ decreases to nearly zero, which is expected as vertical mixing is suppressed. For strongly stable conditions with $\gamma > 0.01$ K m^{-1}, $\overline{w'w'}$ stays very small, except for the two outliers at the FINO1 mast. A similar relationship is found for the comparison of γ and the turbulence intensity I. For the parameters e and γ, the correlation is significantly weaker ($r = -22$ %, see Tab 4). Also, the correlation of $\overline{w'w'}$, I, and e with Ri_B is lower (Table 4), even though Ri_B depends on wind-speed measurement(s) as well.

The correlation within the turbulence criteria e, I and $\overline{w'w'}$, is comparably high, which is not surprising, as the variables partially depend on the same input quantities. Especially high is the correlation between e and $\overline{w'w'}$ with $r = 93$ % for FINO1 (Fig. 7b). The horizontal wind components measured by the aircraft have much larger variances compared with the tower data (Fig. 7b), which is expected during (strong) stable conditions. In contrast, the tower
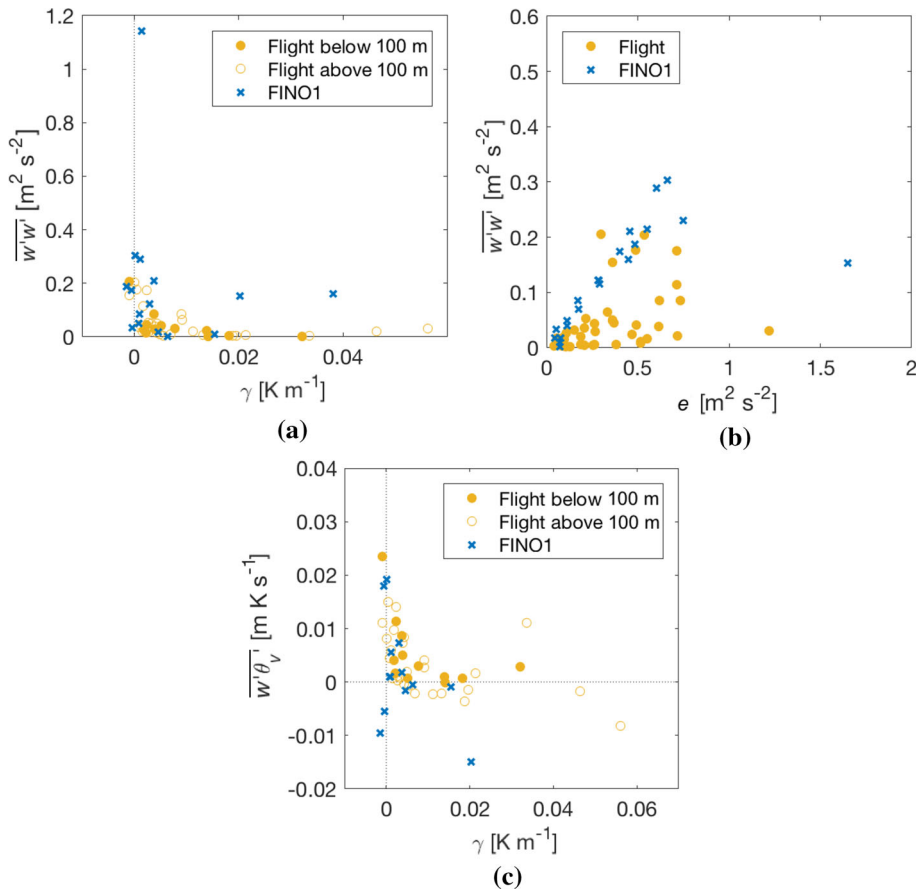
Fig. 7 Scatter plots of different criteria for flight and FINO1 measurements. The turbulence criteria are calculated for the flight leg upstream of the wind farm, which is expected to be in the undisturbed flow and the simultaneously measured 10-min FINO1 data. When the aircraft height deviates from the standard pattern and lies above 100 m, the data point is only indicated as a non-filled marker in the plots that compare aircraft with FINO1 measurements. **a** Variance of vertical velocity component over lapse rate. **b** Variance of vertical velocity component over e. **c** Turbulent kinematic heat flux over lapse rate

data indicate almost isotropic turbulence by a linear correlation, which seems unrealistic for (very) stable cases.

Finally, the stability criteria γ, Ri_B, and ζ are compared with each other: there is a weak correlation between γ and Ri_B. This finding is mainly assigned to outliers in Ri_B and because Ri_B includes wind shear in addition to the thermal stratification of the lapse rate; ζ shows even contradicting correlations with γ and Ri_B in Table 4.

To understand the behaviour, the scatter plot of the turbulent kinematic heat flux $\overline{w'\theta'_v}$–one of the input variables for calculating ζ–is provided in Fig. 7c: for the FINO1 masts no clear statement about the correlation between $\overline{w'\theta'_v}$ and γ can be made as data are very limited. Stable cases especially, which predominately occur for a south-westerly wind (see Sect. 4.1), have been excluded from our dataset, since turbulence measurements (and therefore the turbulence heat flux measurements) by the tower for wind directions of $\phi > 180°$ are not considered. For neutral conditions a strong variation in the heat flux is observable. For

the few stable cases, the heat flux approaches zero, which is expected, apart from the one outlier at $\gamma = 0.01\,\mathrm{K\,m^{-1}}$. For the aircraft data the expected trend is visible: a coincidence of the highest $\overline{w'\theta'_v}$ value with the lowest γ value, and by the trend of a decrease of $\overline{w'\theta'_v}$ with more positive γ ($r = 69\,\%$). However, whereas the vast majority of the samples are classified as stable according to γ, the outcome is reverse for $\overline{w'\theta'_v}$. It is assumed that this result is a consequence of the following:

– As in the case of Ri_B, ζ includes wind shear in addition to the thermal stratification solely in γ, which may cause a major deviation.
– Different measurement heights are considered by the different stability parameters. Whereas γ and Ri_B are obtained within a layer with a vertical separation from 50 to 100 m a.s.l., ζ and one of its input variables $\overline{w'\theta'_v}$ are recorded only at one distinct height at 100 m. In case there are temperature inversions present over the relevant height interval, γ averages over several layers and does not represent the actual temperature gradient, whereas the measure ζ represents the stability of the measurement height (probably) better, but ignores layers below an inversion. An example for that is observed for flight 31 and is discussed in Platis et al. (2020). For some of the presented case studies, this implies that stable inversions closer to the surface are present, leading to the observed majority of positive γ but negative ζ detected at a height aloft.
– When γ is positive, only a negative sensible heat flux is possible, unless, directly above the water a convection layer with an unstable stratification is located, and the heat is transported upwards against the stratification (counter-gradient). This effect could also partially explain the findings in Sect. 4.1.1.

### 4.2.3 Evaluation of Criteria and Implications

In the present dataset, the lapse rate is considered to be the most robust parameter, as there is a good agreement between the airborne data and the FINO tower data especially for near-neutral and slightly stable conditions. The conclusion can be drawn that this study shows good reasons why FINO measurements can be used as a reliable data source for the temperature gradient in the German Bight at the wind farm of interest. However, the disadvantages of the criteria are a high uncertainty when it comes to very stable conditions and when inversions or stable surface layers are present. Moreover, a dry adiabatic lapse rate does not automatically mean neutral conditions, as excess buoyancy and free convection can still be present (Stull 1988). Also in the dataset, an accumulation of the results for near-neutral conditions ($\gamma \approx 0$) is observed, which makes it difficult to distinguish convective cases here.

There are two stability criteria taking the effect of shear-generated turbulence into account: first, Ri_B, whose agreement with the other criteria is weak as outliers lead to an unreliable result. Second, ζ deviates from the static stability, which results in a significantly higher portion of convective cases probably originating in the presence of stable layers below the measurement height of ζ and the additional shear generated turbulence term. The most promising turbulence parameter is $\overline{w'w'}$, showing a functional relationship with the temperature gradient γ. Used as an additional parameter, this variable could support a further classification during situations with a lapse rate close to zero (neutral stratification).

4.3 Airborne Wake Observations

The determination of wakes behind wind farms was possible for 28 out of 41 measurement flights. Those have a meandering pattern of flight legs downstream of the wind farm at hub

Fig. 8 Comparison of the lapse rate derived from the aircraft measurements across the total rotor area (30 to 150 m) with the calculation over alternative height intervals: 50 to 100 m is the interval considered in Sect. 4.2. The interval 60 to 120 m is also centred within the rotor area, but is smaller to improve data availability
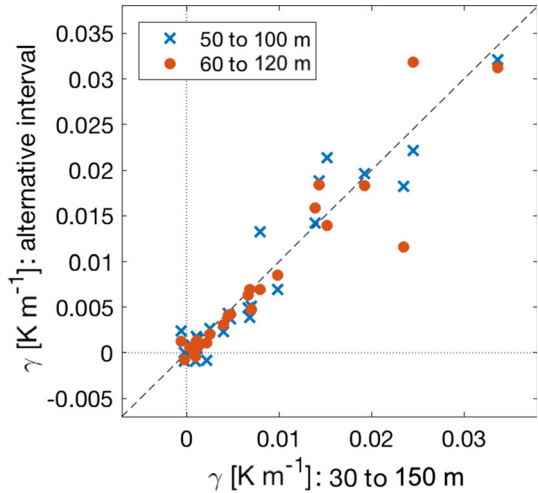
height (Figs. 1 and 2). The remaining 13 flights were excluded due to a different flight strategy. For 12 out of the analyzed flights the wake length, defined as the distance to 95 % recovery, exceeds the length of the meander pattern and for two flights, the wake is observed to be shorter than the first measured leg at hub height. An overview of wake lengths, wake durations, and the initial wind-speed deficit is provided in Table 5.

The observed wakes within the campaign range from nearly zero to over 65 km or exceed 160 min in terms of wake duration. Initial wind-speed deficits D_{r1} approximated at the first downstream leg are observed up to 43 % of the undisturbed flow.

To examine the relationship between wake and stability, the three wake parameters (length x_{95}, wake duration t_{95}, and initial wind-speed deficit D_{r1}) are compared to stability indicators. Based on Sect. 4.2 those are the lapse rate γ and the variance of the vertical velocity component $\overline{w'w'}$.

4.3.1 Height Interval of the Lapse Rate

Since γ depends on the applied height interval (see also Sect. 4.1), the question arises, which is the most representative interval for the wake evolution? For an offshore wind farm, it is likely to be across the total rotor area which is 30–150 m for the Amrumbank West wind farm. A comparison of the flight lapse rate evaluated over different intervals shows good agreement between γ calculated across the rotor area and an alternative smaller interval but also centred within the rotor area of 60–120 m (Fig. 8). As the outcome agrees well for the given case studies, the smaller interval of 60–120 m is used in the following analysis, as it has the advantage of higher data availability and is centred within the rotor area.

For the FINO1 and FINO3 masts, no calculation of an interval centred within the rotor area is possible due to the limited height of the towers. However, the towers have the advantage of measuring the sea-surface temperature. The comparison of γ evaluated over different height intervals (Fig. 9) shows a good linear correlation, especially between the sea surface (0 m) to 30 m and the 0–100 m interval. It also shows that γ measured between 0–100 m has the tendency to be more neutral and this tendency is even enhanced for the 50–100-m interval compared with the 0–30-m interval. The lapse-rate interval close to the ground can be interpreted as an indication of the surface forcing. Hence, with the use of the lowest interval,

Table 5 Overview of wake parameters

AC No	Wind Farm	x_{95} (km)	t_{95} (min)	D_{r1} (%)	x_1 (km)	AC No	Wind Farm	x_{95} (km)	t_{95} (min)	D_{r1} (%)	x_1 (km)
1	AW/MSO/NO	34	83	22	1.6	28	MSO/NO	18	50	10	4.4
2	AW/MSO/NO	22	83	36	4.1	29	AW/MSO/NO	<1	<1	4	0.3
3	AW/MSO/NO	>14	>80	21	1.0	30	MSO	16	31	29	0.7
4	AW	>34	>70	11	4.8	30	NO	22	42	19	0.7
5	AW	14	41	15	3.5	30	AW	39	79	28	0.7
7	AW/MSO/NO	>44	>107	26	4.6	31	MSO	25	31	22	0.8
8	AW/MSO/NO	>24	>85	13	4.0	31	NO	12	14	19	0.8
9	GO	>45	>53	7	1.0	31	AW	53	71	31	0.8
11	GO	1	2	9	0.7	32	AW/MSO/NO	>4	>4	11	2.7
13	GO	35	92	30	1.2	33	AW/MSO/NO	>3	>5	15	2.8
16	GO	7	13	9	2.3	34	AW/MSO/NO	>3	>13	13	3.2
17	GO	<1	<2	5	1.5	35	AW	35	75	14	0.4
20	GO	>35	>163	18	3.0	36	AW	>65	>136	30	0.3
22	GO	>15	>36	12	3.2	37	GO	24	59	24	5.0
24	AW	>54	>123	43	0.5	38	AW	41	75	27	0.5
25	MSO/NO	47	75	–	>5	41	GO	>55	>91	25	0.8
25	AW	51	87	31	0.7						

AC No is the flight number. Wake length x_{95} and duration t_{95} are evaluated at the point of 95% recovery, and D_{r1} is the initial wind-speed deficit measured at the distance x_1 downstream of the wind farm

Fig. 9 Comparison of the lapse rate γ measured at the FINO masts during the flight times evaluated over different height intervals
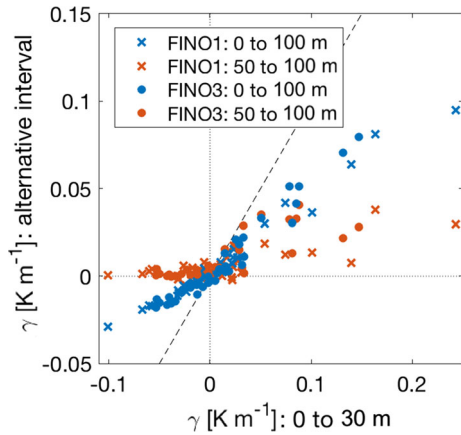
the best representation of convective cases is achieved. This is important to account for any neutrally stratified layer located at higher altitudes, but may be still convective due to a strong surface forcing by a large surface sensible heat flux (Stull 1988). Therefore, the lapse rate is calculated from the sea surface to the lowest temperature reading on the mast to explicitly include the surface forcing in contrast to the aircraft measurements (with an interval between 60 and 120 m) in the further analysis of the correlation between the wake length and stability.

4.3.2 Comparison of Wake and Stability

The comparison of the wake parameters (wake parameters length x_{95}, wake duration t_{95}, and initial wind-speed deficit D_{r1}) with the lapse rate γ evaluated from the aircraft measurement is provided in Fig. 10. A common trend is not very clear regarding all wind-farm clusters at once. When looking at a distinct wind-farm clusters, the trend towards longer wakes with stronger stability for the Godewind and Amrumbank West wind-farms is observed. This trend is revealed by a function of the form

$$\gamma = a_1 (x_{95})^{a_2} - a_3. \tag{10}$$

In terms of wake duration (Fig. 10b), a trend of longer wake duration is only visible for the Godewind observations (blue filled dots). For the other wind farms there is no clear correlation in our data. Comparing the initial wind-speed deficit with γ (Fig. 10c) indicates that small deficits occur during more convective conditions, assuming the Godewind measurement point of flight 9 with a gradient of $0.03 \, \mathrm{K \, m^{-1}}$ to be an outlier. In contrast, with higher initial deficits, the range of stability widens. During strong stability, large D_{r1} values are observed, supporting the hypothesis that wake effects within the wind farm are more pronounced during stable conditions. Excluding the outlier of flight 9, a linear regression with a slope of $5 \times 10^{-4} \, \mathrm{K \, m^{-1}}$ approximates the behaviour.

By comparing the wake length with the values of γ evaluated at the FINO1 and FINO3 masts (from 0 to 30 m), a similar correlation to the aircraft observations is possible (Fig. 11a).

The overall trend is that the wake length increases with stability and especially no short wakes are present during very stable conditions. For visualization, a regression with a r.m.s.e. of $0.05 \, \mathrm{K \, m^{-1}}$ and the form of $\gamma = 3.2 \times 10^{-5} \times (x_{95})^{2.8} - 0.036$ for γ in $\mathrm{K \, m^{-1}}$ and x_{95} in metres is fitted to all wake measurements that captured the whole wake dissipation (filled markers).
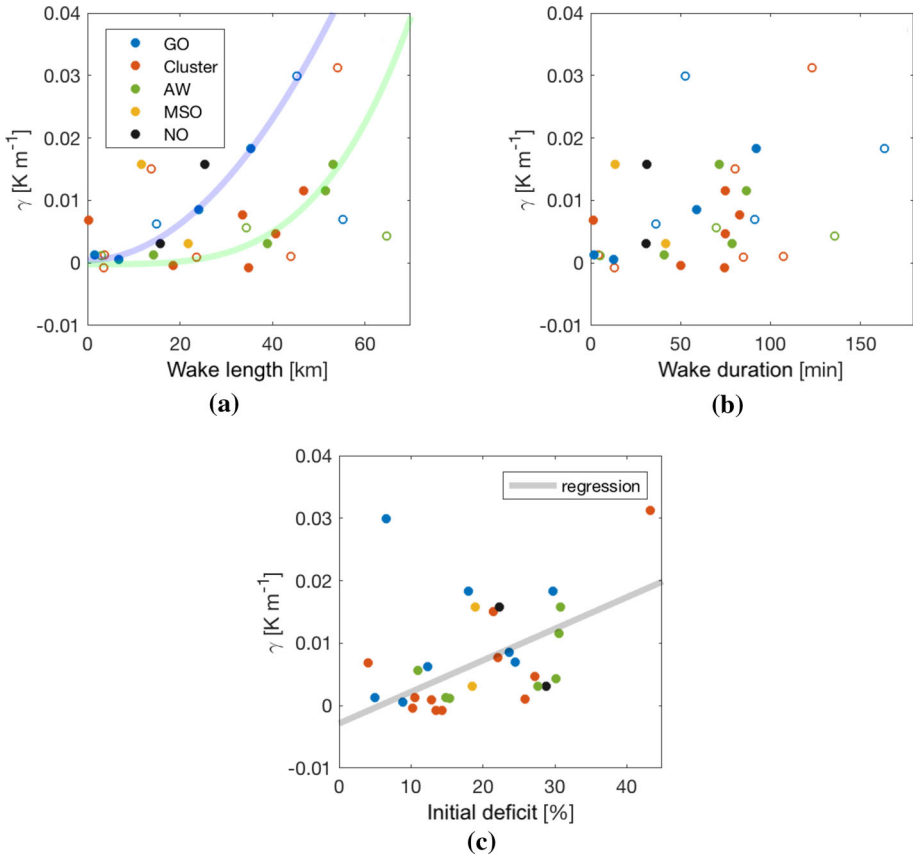
Fig. 10 Scatter plots of wake length x_{95}, duration t_{95}, initial wind-speed deficit D_{r1} and static stability obtained from the flight measurements. The respective wind farm is colour coded. Observations of one common wake downwind of Amrumbank West cluster or Nordsee Ost and Meerwind Süd-Ost are assigned as "Cluster". An empty marker indicates the minimum wake extension if the wake exceeds the meander pattern. **a** Lapse rate versus x_{95} and regression for Godewind (blue line) and AW (green line) data. Figure adapted from Platis et al. (2021). The regressions have the form for Godewind: $\gamma = 1.6 \times 10^{-5} \times (x_{95})^{2.0} - 4.6 \times 10^{-4}$ and AW: $\gamma = 7.4 \times 10^{-5} \times (x_{95})^{3.6} - 1.9 \times 10^{-4}$ with γ in $\mathrm{K\,m^{-1}}$ and x_{95} in metres. **b** Same as in Fig. 10a but for the wake duration t_{95}. **c** D_{r1} and linear regression with $\gamma = 5 \times 10^{-4}\,\mathrm{K\,m^{-1}}\ y_0 - 0.003\,\mathrm{K\,m^{-1}}$

A comparison of wake length and vertical velocity variance $\overline{w'w'}$ shows no clear relationship (Fig. 11b) for all wind farms. However, considering wake measurements only downwind of Godewind, there is an indication that the value of $\overline{w'w'}$ reduces with the increase in wake length. The same trend is observed for the wake duration (not shown here). We tested the correlation with the other parameter such as e, I, or ζ, too. For these stability and turbulence criteria no clear correlation for the entire dataset as well as for individual wind farms is found (not shown).

In summary, a distinct correlation between wakes and stability is complex to define:

– A correlation is seen for the initial wind-speed deficit and the thermal stability γ. Higher wind-speed deficits and longer wakes are observed during more stable conditions.
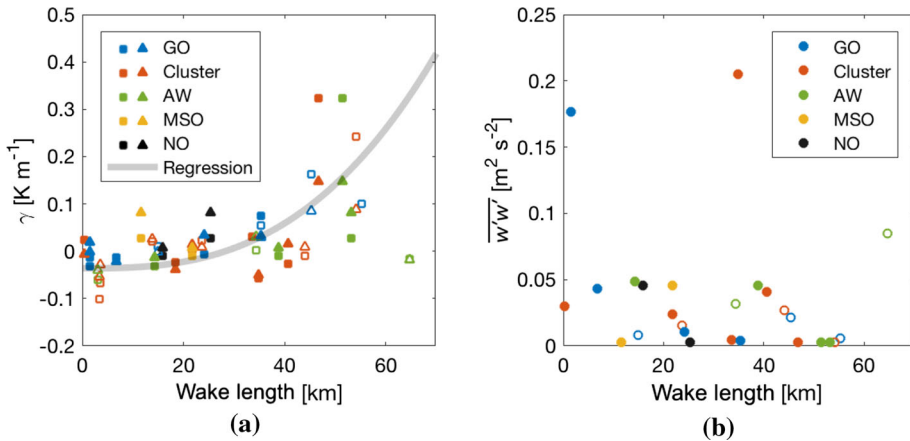– Strong stability coincides with the absence of short wakes.

Fig. 11 Scatter plots of wake length over the FINO lapse rate obtained from the FINO1 (squares) and FINO3 (triangles) and secondly over the variance of vertical velocity components $\overline{w'w'}$ from the aircraft measurement. The according wind farm is colour coded and an empty marker indicates the minimum wake extension if the wake exceeds the meander pattern. The regression in (**a**) has the form of $\gamma = 3.2 \times 10^{-5} \times (x_{95})^{2.8} - 0.036$ with γ in $K\,m^{-1}$ and x_{95} in m. **a** Lapse rate at FINO1 (squares) and FINO3 (triangles) over x_{95}. **b** $\overline{w'w'}$ over x_{95}

– For wakes from individual wind farms, such as Godewind or Amrumbank West, small values of $\overline{w'w'}$ and thermal stability correlate with longer wakes.

We conclude that the relationship cannot be expressed simply in a clear correlation of stability and wake. Further, superimposed effects, which are not assessed here, make the picture indistinct. Besides uncertainties in the method for a representative stability and wake determination, the farm architecture could be an additional factor which impacts the result. Platis et al. (2020) showed that wake lengths downstream of the wind farm Amrumbank West–with a very dense turbine spacing–are much longer than wakes from the neighbouring wind farm Nordsee Ost or Meerwind Süd-Ost with much sparser turbine spacing, despite identical atmospheric conditions.

5 Conclusion

The lapse rate γ calculated using the FINO towers and airborne measurements are in good agreement for simultaneous measurements in the German Bight. A statistical error of $0.008\,K\,m^{-1}$ is found between the FINO data compared to the flight measurements close to the wind farm of interest, although there is a spatial separation of several of 10 km between the measurements. Therefore, γ is considered as a robust parameter describing stability for a region such as the German Bight.

On the contrary, a comparison of turbulence measurements at FINO1 and aboard the aircraft is evaluated as less consistent, probably due to the influence of adjacent wind farms on FINO1, as noted by Foreman et al. (2017), and the different altitudes where turbulence measurements were available. Especially, comparing gradient-based approaches over a layer of several of dozens of metres and turbulence measurements at one certain height leads to differences. A main reason is temperature inversions inside these layers or below the observed measurement heights, as discussed in more detail in Platis et al. (2020).

The study supports the hypothesis that static stability in the German Bight depends on the wind direction, and stable conditions are predominantly expected for flow from the land from the south to south-west and south-east. In addition, the evaluation of the stability depends on the measurement height. In the German Bight, by trend, a near-surface (0 to 30 m), predominantly convective layer is present and more stable conditions are found aloft. Using the highest altitude interval (55 to 95 m), stable conditions are found for 88 % of the investigated cases, whereas extending the interval down to the sea surface results in only 29% of cases being stable for the FINO3 mast. Therefore, it is crucial to consider the height of the boundary layer and possible inversions in the temperature profile when evaluating stability.

The comprehensive analysis of 28 airborne in situ measurements downwind of the wind farms Godewind and the Amrumbank West cluster mainly under thermally stable conditions, reveals wake lengths of more than 65 km. The length at which the wind speed inside the wake has recovered to 95 % of the free stream characterizes the maximum length of the wake. The initial wind-speed deficit D_{r1} is found to range up to 43 % compared with the undisturbed flow, which supports the finding of the previous analyses by Platis et al. (2018), Cañadillas et al. (2019), Platis et al. (2020), and Platis et al. (2021). However, in this study all flights of the WIPAFF campaign have been considered now, leading to more representative results.

Our data analysis reveals that there is a trend of longer wake lengths with stronger atmospheric stability, which is expected from the results of analytical models such as that proposed by Emeis (2010). However, the correlation is not clear if wakes are observed not only during strongly stable cases, but also during near-neutral conditions. Apart from the impact of possible temperature inversions, this variance in the data indicates that under the investigated thermally stable conditions, the wake intensity is influenced by further factors. Those could be for example, the operating state of the wind farms, wind-turbine dimensions, or the farm layout (its width, the angle of incident flow or turbine spacing). The latter is supported by the findings from recent studies such as Kühn and Schneemann (2017) and Platis et al. (2020). Hypothesizing that the wind-farm layout is one of the main drivers for controlling the wake length under statically stable conditions, this would attribute farm architecture a high relevance in planning new farms, since, as is the case in the German Bight, stability varies with wind direction.

Appendix

Table 6 Overview about flight and stability criteria part 1

AC No	Date YYYY/mm/dd	Take off in UTC	Landing in UTC	Wind Farm	U (m s^{-1})	ϕ (°)	γ in K(100 m)$^{-1}$ AC	FINO1	FINO3
1	2016/09/06	1154	1524	AW	7.0	198	0.56	0.12	
2	2016/09/07	0721	1046	AW	5.9	202	1.39	0.81	1.54
3	2016/09/07	1156	1401	AW	4.0	190	1.68	− 0.06	1.87
4	2016/09/08	0823	1226	AW	8.9	131	0.78	0.14	0.50
5	2016/09/09	0853	1242	both	7.0	227	0.43	− 0.19	0.37
6	2016/09/09	1329	1712	AW	6.8	243	0.40	− 0.18	− 0.07
7	2016/09/10	0733	1115	AW	8.5	191	0.18	0.25	0.25
8	2016/09/10	1210	1560	AW	5.0	171	0.22	− 0.18	0.46
9	2017/03/30	1341	1703	GO	17.7	242	4.63	3.80	3.29
10	2017/03/31	1327	1701	GO	13.0	180			
11	2017/04/05	1335	1634	GO	13.9	299	0.91		0.24
12	2017/04/06	1321	1623	GO	10.5	301	0.32		0.38
13	2017/04/09	1028	1406	GO	7.2	213	1.96		2.88
14	2017/04/09	1636	1719	GO	5.6	188	3.36		3.53
15	2017/04/11	0916	1310	GO	7.9	281	0.27		0.11
16	2017/04/11	1402	1709	GO	7.3	258	0.11		0.36
17	2017/04/13	1124	1445	GO	13.4	292	0.05		0.31
18	2017/05/17	1126	1428	AW	6.7	114	2.13		3.25
19	2017/05/17	1503	1802	AW	10.2	121	5.62	5.07	2.08
20	2017/05/23	0742	1042	GO	3.8	252	1.88	2.13	1.71
21	2017/05/23	1113	1512	GO	11.7	301	0.27	− 0.15	0.06
22	2017/05/24	0536	0935	GO	6.8	289	0.49	0.58	0.55
23	2017/05/24	1006	1411	GO	8.8	274	0.43	0.46	0.48
24	2017/05/27	0835	1158	AW	10.0	151	3.21	3.24	3.99
25	2017/05/27	1231	1636	AW	11.9	131	1.82	4.59	2.52
26	2017/05/31	0851	1147	GO	10.6	287	0.16	0.10	0.03
27	2017/05/31	1250	1650	GO	8.7	309	0.08	0.08	0.01
28	2017/06/01	0702	1054	AW	6.8	306	− 0.09	− 0.53	− 0.04
29	2017/06/02	0647	1040	AW	3.5	145	0.39	1.75	− 0.61
30	2017/08/08	0834	1233	AW	7.6	85	0.23	0.31	0.44
31	2017/08/08	1259	1707	AW	12.8	79	1.42	0.89	1.31
32	2017/08/09	0825	1237	AW	15.9	215	0.24	0.12	0.15
33	2017/08/09	1302	1705	AW	12.9	240	0.18	0.28	0.11
34	2017/08/10	1043	1455	AW	4.6	321	0.00	0.02	0.30
35	2017/08/14	1224	1409	AW	7.7	142	− 0.09	0.40	0.13
36	2017/08/14	1431	1832	AW	6.8	115	0.38	0.47	0.09
37	2017/08/15	0719	1116	GO	6.7	189	0.69	0.29	0.16

Table 6 continued

AC No	Date YYYY/mm/dd	Take off in UTC	Landing in UTC	Wind Farm	U (m s^{-1})	ϕ (°)	γ in K$(100\,\text{m})^{-1}$		
							AC	FINO1	FINO3
38	2017/08/17	0601	1010	AW	9.7	152	0.51	0.60	0.29
39	2017/10/14	1255	1642	GO	15.3	250	0.91	0.02	0.33
40	2017/10/15	0701	1111	GO	14.2	199	1.13	1.06	0.47
41	2017/10/15	1142	1552	GO	11.4	191	1.32	1.44	0.73

The wind farm is either classified as Godewind meaning the flight is conducted at Godewind or Amrumbank West when it is conducted at the Amrumbank West cluster, AC stands for aircraft measurement, and F1 and F3 abbreviate FINO1 and FINO3. The height intervals for the lapse rate calculation for AC and FINO is between 50 and 100 m. The parameters U and ϕ are evaluated over the vertical flight profiles as median of all values with a height $99\,\text{m} < z < 101\,\text{m}$

Table 7 Overview about flight and stability criteria part 2; AC abbreviates the aircraft measurements and F1 and F3 abbreviate FINO1 and FINO3

AC No	Ri_B			ζ			e (m² s⁻²)		$\overline{w'w'}$ (m⁻² s⁻²)		I (%)	
	AC	F1	F3	AC ζ	AC z	F1 ζ	AC	F1	AC	F1	AC	F1
1	0.4	0.4		0.55	104	−1.03	0.21	0.10	0.005	0.037	5.8	5.9
2	0.9	6.8	0.3	−0.44	90	0.22	0.47	0.06	0.024	0.011	4.8	5.8
3	1.2	−0.8	6.5			−0.86		0.10		0.027		8.7
4	0.9	369	1.4	−3.01	91	−0.13	0.15	0.47	0.031	0.170	4.7	18.1
5	2.3	−0.9	7.2	−2.29	105	0.11	0.36	0.38	0.049	0.162	9.6	7.8
6	1.3	−0.5	0.0	−8.81	275	−0.44	0.62	0.27	0.039	0.119	8.7	9.2
7	−0.1	1.6	0.0	−1.85	92	−1.23	0.11	0.20	0.027	0.071	3.8	5.7
8	3.0	−0.9	0.1	−7.47	90	−0.86	0.10	0.26	0.015	0.096	7.5	10.5
9	1.7	0.9	0.2	1.27	124	−3.64	0.72	0.34	0.022	0.128	3.0	3.8
10						−2.34		0.49		0.116		6.7
11	0.2		0.1	−1.20	242	−0.65	0.33	0.68	0.064	0.241	4.3	6.6
12	−24.3		0.1	−0.68	245	0.04	0.36	0.28	0.050	0.104	6.7	6.0
13	1.0		0.4	36.50	121	−4.61	0.25	0.06	0.004	0.019	7.6	4.3
14	241.1		0.7	−9.89	120	−3.38	0.38	0.04	0.005	0.007	14.7	3.6
15	7.4		0.4	−8.07	247	0.17	0.06	0.19	0.017	0.080	2.8	6.3
16	0.1		0.2	−3.01	120	0.00	0.26	0.41	0.043	0.136	7.3	7.0
17	0.0		0.3	−0.58	118	−0.06	0.49	0.68	0.177	0.242	5.2	6.5
18	1.1		15.5	−27.32	215		0.26		0.006		4.1	
19	3.0	0.9	1.1	2.15	214	−0.06	1.22	1.27	0.030	0.467	5.7	17.0
20	6.4	214	2.2	105.37	248	−0.36	0.04	0.32	0.003	0.037	4.2	7.5

Table 7 continued

AC No	Ri_B AC	F1	F3	ζ AC ζ	AC z	F1 ζ	e (m² s⁻²) AC	F1	$\overline{w'w'}$ (m⁻² s⁻²) AC	F1	I (%) AC	F1
21	0.3	−0.1	1.6	−0.21	122	0.44	0.22	0.43	0.052	0.139	3.9	6.5
22	0.3	13.4	0.5	−17.79	126	−1.67	0.51	0.05	0.008	0.007	11.7	4.2
23	0.4	51.5	0.2	0.35	243	−1.42	0.55	0.10	0.016	0.023	8.3	4.6
24	4.0	2.1	5.5	−6.03	95	−0.09	0.13	1.11	0.002	0.414	2.7	17.7
25	4.0	27.5	1.4	−19.68	92	−0.12	0.09	1.22	0.003	0.498	2.8	16.9
26	0.2	66.2	0.2	−3.52	248	0.03	0.19	0.19	0.020	0.075	4.0	5.9
27	0.0	0.3	0.1	−7.38	248	0.06	0.21	0.17	0.036	0.061	4.6	5.8
28	−0.2	−58.2	−26.0	−10.39	217	1.12	0.36	0.09	0.155	0.051	9.0	11.5
29	1.6	12.1	−3.9	−17.99	94	−0.17	0.27	0.23	0.030	0.086	17.1	18.7
30	0.3	31.8	1.0	−4.34	95	−0.30	0.37	0.43	0.045	0.181	7.9	7.0
31	0.1	0.4	0.3	9.99	93	−0.48	0.10	1.37	0.003	0.471	2.7	12.5
32	2.6	2.7	0.6	−2.35	217	−0.03	0.71	1.37	0.175	0.488	4.4	8.9
33	0.2	15.4	0.6	−1.62	217	0.34	0.71	0.57	0.114	0.236	6.3	7.0
34	0.1	6.6	4.1	−5.32	216	1.50	0.53	0.30	0.204	0.169	15.2	8.3
35	−0.3	1.1	1.2	−2.66	93	0.08	0.30	1.26	0.205	0.504	5.3	22.2
36	0.4	21.1	0.6	−0.94	99	0.00	0.73	2.70	0.085	1.406	12.1	28.0
37	1.8	1.6	0.9	3.29	125	−2.69	0.52	0.09	0.011	0.026	5.2	5.7
38	0.3	4.9	0.7	−0.19	90	−0.33	0.49	0.73	0.041	0.289	5.9	11.0
39	0.1	0.0	0.2	−23.26	250	−0.45	0.62	0.73	0.085	0.300	5.4	6.9
40	0.5	2.1	0.1	4.48	246	−1.33	0.10	0.36	0.020	0.144	1.7	5.9
41	0.5	0.6	0.1	5.70	120	−0.70	0.19	0.47	0.006	0.198	4.9	6.8

The height intervals for the Ri_B calculation for the AC and FINO data is between 50 and 100 m. For the parameter ζ, the measurement height z in m during the flight measurement is added for completion

References

Archer CL, Colle BA, Veron DL, Veron F, Sienkiewicz MJ (2016) On the predominance of unstable atmospheric conditions in the marine boundary layer offshore of the US Northeastern coast. J Geophys Res Atmos 121:8869–8885

Argyle P, Watson SJ (2014) Assessing the dependence of surface layer atmospheric stability on measurement height at offshore locations. J Wind Eng Ind Aerodyn 131:88–99

Balsley BB, Svensson G, Tjernström M (2008) On the scale-dependence of the gradient Richardson number in the residual layer. Boundary-Layer Meteorol 127:57–72

Bärfuss K, Hankers R, Bitter M, Feuerle T, Schulz H, Rausch T, Platis A, Bange J, Lampert A (2019). In-situ airborne measurements of atmospheric and sea surface parameters related to offshore wind parks in the German Bight. https://doi.org/10.1594/PANGAEA.902845

Barthelmie RJ, Jensen L (2010) Evaluation of wind farm efficiency and wind turbine wakes at the Nysted offshore wind farm. Wind Energy 13(6):573–586

Barthelmie RJ, Pryor SC, Frandsen ST, Hansen KS, Schepers J, Rados K, Schlez W, Neubert A, Jensen L, Neckelmann S (2010) Quantifying the impact of wind turbine wakes on power output at offshore wind farms. J Atmos Ocean Technol 27(8):1302–1317

Bodini N, Lundquist JK, Kirincich A (2019) US east coast lidar measurements show offshore wind turbines will encounter very low atmospheric turbulence. Geophys Res Lett 46(10):5582–5591

Camuffo D (2014) Microclimate for cultural heritage, 2nd edn. Elsevier, Boston. https://doi.org/10.1016/B978-0-444-63296-8.00008-1

Cañadillas B, Muñoz-Esparza D, Neumann T (2011) Fluxes estimation and the derivation of the atmospheric stability at the offshore mast FINO1. Sea 41:5

Cañadillas B, Foreman R, Barth V, Platis A, Siedersleben SK, Bange J, Lampert A, Bärfuss K, Hankers R, Schulz-Stellenfleth J, Djath B, Emeis S, Neumann T (2019) Offshore wind farm wake recovery: Airborne measurements and its representation in engineering models. Wind Energy. https://doi.org/10.1002/we.2484

Christiansen MB, Hasager CB (2005) Wake effects of large offshore wind farms identified from satellite SAR. Remote Sens Environ 98:251–268

Corsmeier U, Hankers R, Wieser A (2001) Airborne turbulence measurements in the lower troposphere onboard the research aircraft Dornier 128–6, D-IBUF. Meteorol Z 10:315–329

Djath B, Schulz-Stellenfleth J, Cañadillas B (2018) Impact of atmospheric stability on X-band and C-band synthetic aperture radar imagery of offshore windpark wakes. J Renew Sustain Energy 10(043):301

Emeis S (2010) A simple analytical wind park model considering atmospheric stability. Wind Energy 13(5):459–469

Emeis S (2018) Wind energy meteorology: atmospheric physics for wind power generation. Springer, Berlin

Emeis S, Siedersleben S, Lampert A, Platis A, Bange J, Djath B, Schulz-Stellenfleth J, Neumann T (2016) Exploring the wakes of large offshore wind farms. J Phys Conf Ser 753(092):014

Foreman R, Cañadillas B, Neumann T, Emeis S (2017) Measurements of heat and humidity fluxes in the wake of offshore wind turbines. J Renew Sustain Energy 9(053):304

Frühmann R (2016) Relative calibration process for long term thermal stratification measurements in the lower atmospheric boundary layer. DEWI Mag 48

Hansen KS, Barthelmie RJ, Jensen LE, Sommer A (2012) The impact of turbulence intensity and atmospheric stability on power deficits due to wind turbine wakes at horns rev wind farm. Wind Energy 15:183–196

Henderson AR, Morgan C, Smith B, Sørensen HC, Barthelmie RJ, Boesmans B (2003) Offshore wind energy in Europe-a review of the state-of-the-art. Wind Energy 6:35–52

Krishnamurthy R, Reuder J, Svardal B, Fernando HJS, Jakobsen JB (2017) Offshore wind turbine wake characteristics using scanning Doppler lidar. Energy Procedia 137:428–442

Kühn M, Schneemann J (2017) Analyse der Abschattungsverluste und Nachlaufturbulenzcharakteristika großer Offshore-Windparks durch Vergleich von" alpha ventus" und "Riffgat" ("GW Wakes"): Abschlussbericht des Verbund-Forschungsprojekts: Laufzeit: 01.08. 2011-30.09. 2016; RAVE, Research at Alpha Ventus, eine Forschungsinitiative des Bundesumweltministeriums-Teilprojekt A durchgeführt im Rahmen von RAVE. ForWind-Carl von Ossietzky Universität Oldenburg

Lampert A, Bärfuss KB, Platis A, Siedersleben SK, Djath B, Cañadillas B, Hankers R, Bitter M, Feuerle T, Schulz H, Rausch T, Angermann M, Schwithal A, Bange J, Schulz-Stellenfleth J, Neumann T, Emeis S (2020) In-situ airborne measurements of atmospheric and sea surface parameters related to offshore wind parks in the German Bight. Earth Syst Sci Data

Magnusson M, Smedman AS (1994) Influence of atmospheric stability on wind turbine wakes. Wind Eng 139–152

Muñoz-Esparza D, Cañadillas B, Neumann T, Van Beeck J (2012) Turbulent fluxes, stability and shear in the offshore environment: Mesoscale modelling and field observations at FINO1. J Renew Sustain Energy 4(6): 063–136

Nygaard NG (2014) Wakes in very large wind farms and the effect of neighbouring wind farms. J Phys Conf Ser 524(1): 12,162

Nygaard NG, Hansen SD (2016) Wake effects between two neighbouring wind farms. In: Journal of physics: conference series, IOP Publishing, vol 753, p 032020

OpenStreetMap (2017) Land polygones retrieved from http://openstreetmapdata.com/data/land-polygons. https://www.openstreetmap.org

Peña A, Réthoré PE, Rathmann O (2014) Modeling large offshore wind farms under different atmospheric stability regimes with the park wake model. Renew Energy 70:164–171

Platis A, Siedersleben SK, Bange J, Lampert A, Bärfuss K, Hankers R, Cañadillas B, Foreman R, Schulz-Stellenfleth J, Djath B et al (2018) First in situ evidence of wakes in the far field behind offshore wind farms. Sci Rep 8:2163

Platis A, Hundhausen M, Siedersleben SK, Lampert A, Bärfuss K, Schulz-Stellenfleth J, Djath B, Emeis S, Neumann T, Cañadillas B, Bange J (2020) Long-range modifications of the wind field by offshore wind parks-results of the project WIPAFF. Meteorol Z (Contr Atm Sci) 29:355–376. https://doi.org/10.1127/metz/2020/1023

Platis A, Hundhausen M, Mauz M, Siedersleben S, Lampert A, Bärfuss K, Djath B, Schulz-Stellenfleth J, Canadillas B, Neumann T et al (2021) Evaluation of a simple analytical model for offshore wind farm wake recovery by in situ data and weather research and forecasting simulations. Wind Energy 24(3):212–228

Rhodes ME, Lundquist JK (2013) The effect of wind-turbine wakes on summertime US midwest atmospheric wind profiles as observed with ground-based doppler lidar. Boundary-Layer Meteorol 149(1):85–103

Sachs L (2013) Angewandte statistik: Anwendung statistischer Methoden. Springer

Sathe A (2010) Atmospheric stability and wind profile climatology over the north sea: Case study at egmond aan zee. In: 3rd EWEA Conference-Torque 2010: The Science of making Torque from Wind, Heraklion, Crete, Greece, 28–30 June 2010, European Wind Energy Association

Siedersleben SK, Lundquist JK, Platis A, Bange J, Bärfuss K, Lampert A, Cañadillas B, Neumann T, Emeis S (2018) Micrometeorological impacts of offshore wind farms as seen in observations and simulations. Environ Res Lett 13:124012

Stull RB (1988) An introduction to boundary layer meteorology. Springer

Türk M, Emeis S (2010) The dependence of offshore turbulence intensity on wind speed. J Wind Eng Ind Aerodyn 98(8–9):466–471

Van Wijk A, Beljaars A, Holtslag A, Turkenburg W (1990) Evaluation of stability corrections in wind speed profiles over the North Sea. J Wind Eng Ind Aerodyn 33:551–566

Westerhellweg A, Canadillas B, Beeken A, Neumann T (2010) One year of LiDAR measurements at FINO1-Platform: comparison and verification to met-mast data. In: Proceedings of 10th German wind energy conference DEWEK, pp 1–5

Wharton S, Lundquist JK (2010) Atmospheric stability impacts on power curves of tall wind turbines-an analysis of a west coast north american wind farm. Lawrence Livermore National Laboratory (LLNL), Livermore, CA, Techical report

Wharton S, Lundquist JK (2012) Atmospheric stability affects wind turbine power collection. Environ Res Lett 7(014):005